Substrate Surface Energy Dependent Morphology and Dewetting in an ABC Triblock Copolymer Film

Thomas H. Epps, III,* Dean M. DeLongchamp, and Michael J. Fasolka*

Polymers Division, National Institute of Standards and Technology, Gaithersburg, Maryland 20899

Daniel A. Fischer

Ceramics Division, National Institute of Standards and Technology, Gaithersburg, Maryland 20899

Erin L. Jablonski

Department of Chemical Engineering, Bucknell University, Lewisburg, Pennsylvania 17837

A gradient combinatorial approach was used to examine the effect of substrate surface energy on the morphology and stability of films of a poly(isoprene-*b*-styrene-*b*-ethylene oxide) triblock copolymer that exhibits an alternating gyroid morphology in the bulk. Atomic force microscopy data across our surface energy (water contact angle) library suggest a transformation to predominantly surface parallel lamellae with an antisymmetric ordering. For substrate water contact angles below 70° the film exhibited autophobic dewetting from an adsorbed half-period triblock copolymer monolayer at longer annealing times. X-ray photoelectron spectroscopy and near edge X-ray absorption fine structure analysis along gradient specimens indicated that the substrate surface energy governed the composition profile of the monolayer, and this variation in chemical expression was key to whether the film was stable or autophobically dewet. These observations demonstrate that enthalpic interactions, in addition to entropic considerations, can play a major role in autophobic dewetting of block copolymer films.

I. Introduction

Block copolymers provide the opportunity to design nanostructured materials, the self-assembly of which can be tuned by molecular parameters such as overall molecular mass, constituent volume fractions, and segmental interaction parameters.[1,2] In this sense, linear ABC triblock copolymers, which consist of three polymer species, are particularly promising, since they offer a morphological and chemical diversity not found in diblock copolymer systems. ABC triblocks can form triply periodic and multiply continuous network morphologies, which have superior mechanical attributes relative to their one- and two-dimensional counterparts (lamellae and cylinders)[3] and can potentially be harnessed for advanced technologies, including ion-conduction membranes and templating applications. Three examples of periodic and multiply continuous networks reported in the triblock literature are the core−shell gyroid,[4,5] the orthorhombic (O[70]) network,[6] and the alternating gyroid.[7] In addition to these sightings, all three structures were found in a single ABC triblock phase diagram.[8]

The same diversity that makes ABC triblock copolymers compelling also increases the number and complexity of factors that govern their behavior, and much of this parameter space remains uncharted. In particular, while strides have been made in understanding the bulk phase behavior of ABC triblock copolymers,[9−13] little is known about their thin film behavior. Indeed, with the exception of a few notable studies,[14−16] experimental observations of ABC triblock behavior in thin film geometries are sparse, and fundamental questions remain. Can the interesting symmetries that ABC triblocks exhibit in the bulk persist in thin films? Or, as illustrated in Figure 1a, do they shift to different motifs? How will parameters and constraints such as thickness, substrate surface energy, and annealing affect the ABC film structure and stability?

As a foray into these matters, we examine how substrate surface energy affects the thin film behavior of a poly(isoprene-*b*-styrene-*b*-ethylene oxide) (ISO) triblock copolymer (Figure 1b). The bulk morphology of the copolymer is alternating gyroid ($I4_132$, Q^{214}), consisting of interpenetrating gyroid nets of poly(isoprene) (PI) and poly(ethylene oxide) (PEO) in a matrix of poly(styrene) (PS).[8,13] To facilitate our study, we employ a

* To whom correspondence should be addressed. E-mail: thepps@udel.edu, mfasolka@nist.gov.

(1) Bates, F. S. *Science* **1991**, *251* (4996), 898−905.

(2) Hadjichristidis, N.; Pispas, S.; Floudas, G. A. *Block Copolymers: Synthetic Strategies, Physical Properties, and Applications*; Wiley-Interscience: Hoboken, NJ, 2003.

(3) Dair, B. J.; Honeker, C. C.; Alward, D. B.; Avgeropoulos, A.; Hadjichristidis, N.; Fetters, L. J.; Capel, M.; Thomas, E. L. *Macromolecules* **1999**, *32* (24), 8145−8152.

(4) Goldacker, T.; Abetz, V. *Macromolecules* **1999**, *32* (15), 5165−5167.

(5) Shefelbine, T. A.; Vigild, M. E.; Matsen, M. W.; Hajduk, D. A.; Hillmyer, M. A.; Cussler, E. L.; Bates, F. S. *J. Am. Chem. Soc.* **1999**, *121* (37), 8457−8465.

(6) Bailey, T. S.; Hardy, C. M.; Epps, T. H., III; Bates, F. S. *Macromolecules* **2002**, *35* (18), 7007−7017.

(7) Suzuki, J.; Seki, M.; Matsushita, Y. *J. Chem. Phys.* **2000**, *112* (10), 4862−4868.

(8) Epps, T. H., III; Cochran, E. W.; Hardy, C. M.; Bailey, T. S.; Waletzko, R. S.; Bates, F. S. *Macromolecules* **2004**, *37*, 7085−7088.

(9) Arai, K.; Kotaka, T.; Kitano, Y.; Yoshimura, K. *Macromolecules* **1980**, *13* (6), 1670−1678.

(10) Riess, G.; Schlienger, M.; Marti, S. *J. Macromol. Sci., Phys.* **1980**, *B17* (2), 355−374.

(11) Auschra, C.; Stadler, R. T. *Macromolecules* **1993**, *26*, 2171−2174.

(12) Breiner, U.; Krappe, U.; Thomas, E. L.; Stadler, R. *Macromolecules* **1998**, *31* (1), 135−141.

(13) Epps, T. H., III; Cochran, E. W.; Bailey, T. S.; Waletzko, R. S.; Hardy, C. M.; Bates, F. S. *Macromolecules* **2004**, *37*, 8325−8341.

(14) Krausch, G.; Magerle, R. *Adv. Mater.* **2002**, *14* (21), 1579−1583.

(15) Rehse, N.; Knoll, A.; Magerle, R.; Krausch, G. *Macromolecules* **2003**, *36* (9), 3261−3271.

(16) Ludwigs, S.; Schmidt, K.; Stafford, C. M.; Amis, E. J.; Fasolka, M. J.; Karim, A.; Magerle, R.; Krausch, G. *Macromolecules* **2005**, *38* (5), 1850−1858.
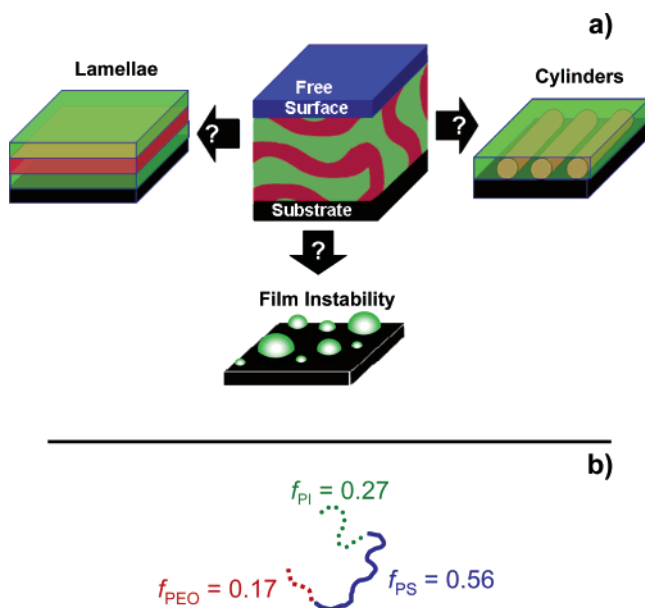
Figure 1. (a) Schematic illustration of the possible effects of free-surface and substrate interactions on the thin film morphology of block copolymers that exhibit triply periodic nanostructures in the bulk. (b) Illustration of the ISO triblock copolymer molecule showing approximate volume fractions.

gradient combinatorial approach similar to that used by Smith et al. to examine films of a symmetric PS-*b*-poly(methyl methacrylate) diblock copolymer[17] and by Ludwigs et al. to study a PS-*b*-poly(2-vinylpyridine)-*b*-poly(*tert*-butyl methacrylate) triblock.[16] Our combinatorial libraries express an extensive range of surface energies on a single substrate and thus provide a comprehensive map of the effect of this parameter on substrate-supported ISO films The ISO thin film structure and surface chemistry are characterized across the library by a variety of methods, including optical microscopy, atomic force microscopy (AFM), X-ray photoelectron spectroscopy (XPS), and near edge X-ray absorption fine structure (NEXAFS) spectroscopy.

When our results are considered, discussed below, two major bodies of previous work provide guidance and background. First, is the extensive literature describing the influence of interfaces on the morphology of diblock copolymer films, which is summarized in two recent review articles.[18,19] In most cases, the substrate (or free) surface drives preferential wetting of the block with the lower interfacial energy (or surface energy), resulting in microdomains that are oriented parallel to the substrate.[18,19] Surface parallel microstructures show two general forms. In "symmetric" systems, the same block resides at both the substrate and free surface, and the surface parallel ordering exhibits a neat A−B/B−A periodicity. "Antisymmetric" systems involve different blocks at the free and substrate surface. In this case, a half-period monolayer resides at the substrate, so the film layering proceeds like B−A/A−B/B−A. If the substrate chemistry is "neutral", i.e., it has no preferential interaction with either block, the domains can orient normal to the substrate interface.[17,20−23]

In the case of ABC triblocks, this situation is expected to be more complex, since the substrate can have favorable interactions with one or multiple blocks.[24,25]

The second body of research concerns film dewetting phenomenon, and two major forms of polymer dewetting have been highlighted in the literature. In the most common scenario, the polymer dewets directly from the substrate surface. This process can occur via different routes but is generally driven by unfavorable *enthalpic* interactions between the substrate and the polymer.[26,27] In the second scenario, polymer films can dewet from a monolayer of material (chemically identical to the film) that is grafted or otherwise attached to the substrate.[28−32] This is called autophobic dewetting or pseudodewetting. As formulated by Liebler for the case of a homopolymer film atop a homopolymer brush of identical composition, autophobic dewetting is typically driven by the lower conformational *entropy* of chains that are grafted (or otherwise adsorbed) to the surface compared to the untethered material in the rest of the film.[33] This entropic driving force for autophobic dewetting in polymer melts is of major importance, as opposed to in small molecule systems where dewetting is typically enthalpy driven.[34,35] Several researchers have observed and examined polymeric autophobic dewetting in a variety of systems.[36−42] For example, Reiter and Sommer[36,39] reported autophobic dewetting in poly(ethylene oxide) films annealed on SiO_2 surfaces. In this system, strong pinning interactions between the polymer and oxide significantly reduced the conformational entropy of chains next to the surface. In this work, the authors noted variations in the rate of dewetting as a function of position. Because no differences in the surface tension in the monolayer could be discerned, they hypothesized that these variations were due to local differences in the strength of surface interaction, which presumably changed the conformational entropy of pinned chains. Liu and co-workers[43] examined autophobic dewetting in PS films deposited on a PS-*b*-poly(2-vinylpyridine) monolayer, which presented a surface of tethered PS chains. In this study, the role of conformational entropy was demonstrated by changing the molecular weight of the PS homopolymer, and dewetting occurred when the length of the free PS chains was much greater than those in the adsorbed

(17) Smith, A. P.; Sehgal, A.; Douglas, J. F.; Karim, A.; Amis, E. J. *Macromol. Rapid Commun.* **2003**, *24* (1), 131−135.

(18) Fasolka, M. J.; Mayes, A. M. *Annu. Rev. Mater. Res.* **2001**, *31*, 323−355.

(19) Segalman, R. A. *Mater. Sci. Eng., R* **2005**, *48* (6), 191−226.

(20) Kellogg, G. J.; Walton, D. G.; Mayes, A. M.; Lambooy, P.; Russell, T. P.; Gallagher, P. D.; Satija, S. K. *Phys. Rev. Lett.* **1996**, *76* (14), 2503−2506.

(21) Huang, E.; Rockford, L.; Russell, T. P.; Hawker, C. J. *Nature* **1998**, *395* (6704), 757−758.

(22) Huang, E.; Russell, T. P.; Harrison, C.; Chaikin, P. M.; Register, R. A.; Hawker, C. J.; Mays, J. *Macromolecules* **1998**, *31* (22), 7641−7650.

(23) Yang, X. M.; Peters, R. D.; Nealey, P. F.; Solak, H. H.; Cerrina, F. *Macromolecules* **2000**, *33* (26), 9575−9582.

(24) Pickett, G. T.; Balazs, A. C. *Macromol. Theory Simul.* **1998**, *7* (2), 249−255.

(25) Ludwigs, S.; Krausch, G.; Magerle, R.; Zvelindovsky, A. V.; Sevink, G. J. A. *Macromolecules* **2005**, *38* (5), 1859−1867.

(26) Reiter, G. *Phys. Rev. Lett.* **1992**, *68* (1), 75−78.

(27) Geoghegan, M.; Krausch, G. *Prog. Polym. Sci.* **2003**, *28* (2), 261−302.

(28) Gay, C. *Macromolecules* **1997**, *30* (19), 5939−5943.

(29) Reiter, G.; Auroy, P.; Auvray, L. *Macromolecules* **1996**, *29* (6), 2150−2157.

(30) Shull, K. R. *Faraday Discuss.* **1994** (98), 203−217.

(31) Yerushalmirozen, R.; Klein, J.; Fetters, L. J. *Science* **1994**, *263* (5148), 793−795.

(32) Wyart, F. B.; Martin, P.; Redon, C. *Langmuir* **1993**, *9* (12), 3682−3690.

(33) Ferreira, P. G.; Ajdari, A.; Leibler, L. *Macromolecules* **1998**, *31* (12), 3994−4003.

(34) Zisman, W. A. Relation of the equilibrium contact angle to liquid and solid construction. In *Contact Angle, Wettability, and Adhesion*; Fowkes, F. M., Ed.; ACS Advances in Chemistry Series; American Chemical Society: Washington, DC, 1964; Vol. 43, pp 1−51.

(35) Degennes, P. G. *Rev. Mod. Phys.* **1985**, *57* (3), 827−863.

(36) Reiter, G.; Sommer, J. U. *Phys. Rev. Lett.* **1998**, *80* (17), 3771−3774.

(37) Hamley, I. W.; Hiscutt, E. L.; Yang, Y. W.; Booth, C. *J. Colloid Interface Sci.* **1999**, *209* (1), 255−260.

(38) Limary, R.; Green, P. F. *Langmuir* **1999**, *15* (17), 5617−5622.

(39) Reiter, G.; Sommer, J. U. *J. Chem. Phys.* **2000**, *112* (9), 4376−4383.

(40) Reiter, G.; Sharma, A. *Phys. Rev. Lett.* **2001**, *871* (16), 166103.

(41) Limary, R.; Green, P. F.; Shull, K. R. *Eur. Phys. J. E* **2002**, *8* (2), 103−110.

(42) MacDowell, L. G.; Muller, M. *J. Phys.: Condens. Matter* **2005**, *17* (45), S3523−S3528.

(43) Liu, Y.; Rafailovich, M. H.; Sokolov, J.; Schwarz, S. A.; Zhong, X.; Eisenberg, A.; Kramer, E. J.; Sauer, B. B.; Satija, S. *Phys. Rev. Lett.* **1994**, *73* (3), 440−443.
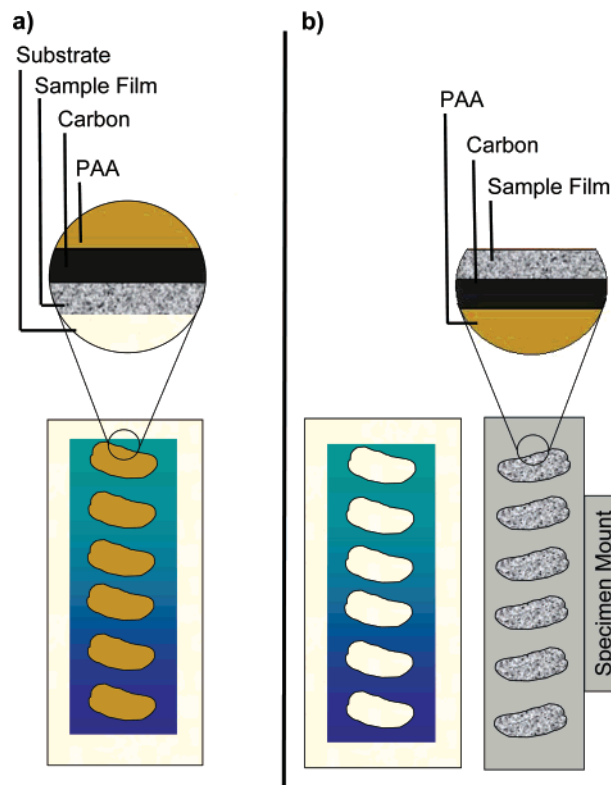
diblock. Green and co-workers provide one of the first and subsequent reports of autophobic dewetting in pure diblock film systems.[38,44] In these works, PS-b-PMMA films dewet from a half-period monolayer residing on an SiO_2 surface, but only when the diblock film was heated above its order−disorder transition temperature. Because the bulk of the film is disordered under these conditions, the phenomenon is qualitatively similar to the case reported by Liu et al. and Hamley et al., who reported autophobic dewetting in ABA triblock films.[37] The common theme in these studies is that no variations in the surface chemistry of the pinned layer are observed (or really even possible), so entropy is necessarily the primary driving factor. As we discuss below, our ISO triblock copolymer films on a surface energy gradient are different in this respect and thus may present a new twist on autophobic dewetting behavior in block copolymer systems. In addition, we observe autophobic dewetting upon annealing at 120 °C, which is slightly below the polymer's bulk order−disorder transition temperature of 124 °C.[13]

II. Experimental Section

Materials. The poly(isoprene-*b*-styrene-*b*-ethylene oxide) (ISO) triblock copolymer examined in this study was synthesized by sequential anionic polymerization at the University of Minnesota. The polymer number average molar mass and volume fractions were $M_n = 14\,500$ g/mol and $f_{PI} = 0.27$, $f_{PS} = 0.56$, and $f_{PEO} = 0.17$, respectively. Detailed synthesis and characterization data for the ISO copolymer studied in this work can be found elsewhere (along with details of the bulk morphology characterization).[8,13] The bulk morphology is an alternating gyroid, with an order−disorder transition temperature of 124 °C and a bulk domain spacing of 22 nm.[13]

Fabrication of Substrate Surface Energy Library. Surface energy gradient libraries were produced using previously reported procedures.[45] Silicon wafers (N ⟨100⟩, Wafer World, Inc.)[46] were rinsed with ethanol and conditioned for 40 min in a commercial ultraviolet ozone (UVO) cleaner (model 342-220, Jetlight Co., Inc.) prior to use. The wafers were then exposed to *n*-octyldimethyl-chlorosilane (ODS, Gelest, Inc.) vapor for 6 h to form a self-assembled monolayer (SAM) on the substrate surface. The modified surface was thoroughly washed with toluene and dried. A custom-built motorized stage was employed to translate the coated substrate beneath a UV wand lamp (184.9 and 253.7 nm) projected through a 2 mm wide slit aperture. The SAM was exposed to a UVO radiation gradient by acceleration under the slit; the distance between the substrate and the wand lamp was set to 1 mm, and exposure times were programmed using commercial software (Labview, National Instruments) to ramp from 0.1 to 6 s. Water and diiodomethane static contact angles were measured using a Kruss G2 contact-angle measuring system and converted to surface energies by following established procedures.[17,45] Water contact angles ranging from 90° to 10° (surface energies from 26 to 70 mJ/m²) were generated over a 30 mm region on a single substrate.

Film Specimen Preparation. Uniform thickness triblock films were deposited on the ODS-modified substrate using the flow-coating technique, which is described in the literature.[47,48] In short, this method creates films by spreading a layer of polymer solution over a substrate with a knife blade. Film thickness is determined by the velocity of the knife blade, the polymer solution concentration, the gap between blade and the substrate, and the volume of solution deposited into this gap. For our specimens, 50 μL of a 1.5% by mass

(44) Arceo, A.; Green, P. F. *J. Phys. Chem. B* **2005**, *109* (15), 6958−6962.
(45) Julthongpiput, D.; Fasolka, M. J.; Zhang, W. H.; Nguyen, T.; Amis, E. J. *Nano Lett.* **2005**, *5* (8), 1535−1540.
(46) Certain equipment and instruments or materials are identifed in the paper in order to adequately specify the experimental details. Such identification does not imply recommendation by the National Institute of Standards and Technology, nor does it imply the materials are necessarily the best available for the purpose.
(47) Stafford, C. M.; Roskov, K. E.; Epps, T. H.; Fasolka, M. J. *Rev. Sci. Instrum.* **2006**, *77* (2), 023908.
(48) Meredith, J. C.; Smith, A. P.; Karim, A.; Amis, E. J. *Macromolecules* **2000**, *33* (26), 9747−9756.

Figure 2. Schematic illustration of the film removal technique used to examine the bottom surface of the triblock thin films. (a) A thin carbon buffer layer is sputter-coated on the polymer film. Then, a 25 mass percent poly(acrylic acid) (PAA) in water solution is poured on top of the carbon layer, and the PAA is dried at 50 °C and approximately 50% relative humidity overnight. (b) The film is removed from the substrate using a razor blade under the edges of the hardened PAA, leaving the SAM on the silicon substrate. The film with a PAA/carbon backing is then flipped over and placed on a specimen mount for XPS and NEXAFS analysis.

ISO polymer solution in toluene was spread with knife blade fixed at 200 μm above the substrate surface. Blade velocities were set to achieve film thicknesses of approximately 40 and 9 nm, where thicknesses were measured by AFM scratch tests. Films were 50 mm in length—enough to cover the entire 30 mm surface energy library.

Films were annealed under vacuum in an oven at 120 °C for intervals between 1 and 12 h. Ultimate annealing times were limited due to potential degradation of the PI block. The oven was flushed and back-filled with argon three times immediately after inserting samples. Upon removal from the oven, specimens were immediately quenched on a metal plate.

Analysis of the "bottom" surface of ISO films (i.e., next to the substrate) was achieved by a film-peeling technique that exposed this interface, as illustrated in Figure 2. This process, described in detail elsewhere,[49] involved (1) evaporating a ≈10 nm layer of carbon onto the polymer film, (2) pouring a 25 mass % poly(acrylic acid) (PAA) in water solution on top of the carbon layer, (3) drying the PAA at 50 °C and approximately 50% relative humidity, and (4) removing the polymer film from the silicon/SAM substrate using the PAA/carbon backing as a support. Peeled specimens were transferred to a sample mount (PAA side down) for surface chemical analysis.

Optical and Atomic Force Microscopy. Optical micrographs were acquired with a Nikon Optiphot-2 compound microscope equipped with a CCD camera (JAI CV-S3200). Tapping mode AFM measurements were performed using a Dimension 3100 microscope

(49) Fasolka, M. J.*;* Harris, D. J.; Mayes, A. M.; Yoon, M.; Mochrie, S. G. J. *Phys. Rev. Lett.* **1997**, *79* (16), 3018−3021.

with a Nanoscope IV control unit (Digital Instruments, Inc.). Silicon probes with a nominal spring constant of 40 N/m (NanoDevices, Inc.) were used to image the polymer films.

X-ray Photoelectron Spectroscopy. XPS measurements were carried out using a Kratos Axis 165 spectrometer at a vacuum of 6×10^{-10} Torr with non-monochromatic Mg Kα radiation. The X-ray power was 144 W. Measurements were done in hybrid mode using electrostatic and magnetic lenses, with a step size of 0.1 eV and sweep time of 60 s. All spectra were recorded in the fixed analyzer transmission (FAT) mode with a pass energy of 40 eV and an average of 10 scans for each element analyzed. Binding energies were calibrated with respect to C 1s at 284.6 eV. Data processing was done using Vision processing software (Kratos). After subtraction of a linear background, all spectra were fitted using 60% Gaussian/40% Lorentzian peaks. The fitting parameters were peak position, full width at half-maximum, intensity, and the Gaussian fraction. Initial estimates for binding energy peak locations were based on homopolymer spectra found in the literature.[50] Argon ion etching was conducted for 5 min at an initial argon chamber pressure of 1×10^{-7} Torr.
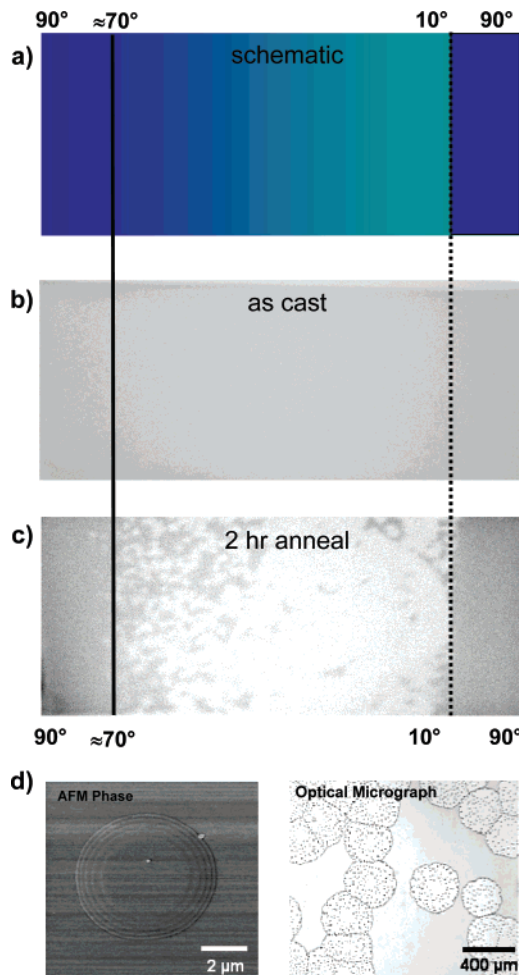
Near Edge X-ray Adsorption Fine Structure Spectroscopy. Near edge X-ray absorption fine structure (NEXAFS) spectroscopy measurements were conducted on the U7A (NIST) material characterization beamline of the National Synchrotron Light Source at Brookhaven National Laboratory. Spectra were collected with the incident beam at the magic angle (54.7°) relative to the sample to remove any polarization dependence of the NEXAFS intensities. The NEXAFS spot size was approximately 1 mm^2. The experimental standard uncertainty in the peak position was ±0.15 eV, and the relative uncertainty in the NEXAFS intensity was less than ±2%.

In a NEXAFS measurement, soft X-rays are preferentially absorbed by the sample when the incident radiation is at the appropriate energy to allow the excitation of a core shell electron of a specific atom (C or O) to an unoccupied molecular orbital. Auger electrons or photons are emitted when the excited core electron decays. By application of a negative voltage entrance grid bias at the partial electron yield detector, electrons of low kinetic energy can be rejected. In this case, a detector bias of −260 V was used to probe the electrons emitted within 1−2 nm of the sample surface. A more detailed description of NEXAFS spectroscopy can be found in the literature.[51]

NEXAFS spectra were fit to a linear combination of PI, PS, and PEO homopolymer spectra acquired using the same detector bias. Fitting was performed using a constrained Levenberg−Marquardt nonlinear least-squares optimization. The homopolymer spectra were baseline (pre-edge) normalized to zero; the sum of the coefficients was typically ≈1, indicating similar photon extinction and electron mean free path for both homopolymer and triblock copolymer samples.

III. Results and Discussion

Figure 3 illustrates our library design and its relationship to the macroscopic ISO film structure observed before and after annealing. As shown in Figure 3a, the surface energy gradient spans substrate water contact angles ($\theta_{w,s}$) from 90° to 10°. A reference region at the rightmost portion of the library retains a $\theta_{w,s} \approx 90°$ because it was not subjected to UVO treatment. Figure 3b shows an ISO film in the as-cast state. This optical image demonstrates that this 40 nm film is stable and continuous across the library. To examine the preannealed film further, AFM analysis was conducted along the library at representative locations. In each case, AFM topography micrographs revealed terraced films with a uniform step height (L_0) ≈ 16 nm, which is slightly compressed relative to the bulk spacing. AFM phase micrographs of similar regions consistently showed a lack of

(50) Beamson, G.; Briggs, D. *High Resolution XPS of Organic Polymers*; John Wiley & Sons: New York, 1992.

(51) Jablonski, E. L.; Prabhu, V. M.; Sambasivan, S.; Lin, E. K.; Fischer, D. A.; Goldfarb, D. L.; Angelopoulos, M.; Ito, H. *J. Vac. Sci. Technol., B* **2003**, *21* (6), 3162−3165.

Figure 3. (a) Schematic illustration of the gradient substrate surface energy library. The total length of the surface energy gradient is 30 mm. The dark blue area to the right of the dashed line depicts where the substrate reverts to $\theta_{w,s} \approx 90°$; this region was used as a reference to ensure library consistency. (b) Optical image of the as cast polymer film. (c) Optical image of same polymer film following 2 h of annealing at 120 °C. Dewetting is observed for $\theta_{w,s} < 70°$. (d) (left) AFM phase micrograph showing featureless terraces, consistent with a surface-parallel lamellar microstructure, observed across the preannealed library and for annealed films where $\theta_{w,s} > 70°$. This image was acquired $\theta_{w,s} \approx 86°$ after 8 h of annealing. (right) Optical micrograph of dewetting film at $\theta_{w,s} \approx 60°$ after 2 h annealing at 120 °C.

lateral nanostructures in these terraces, which is suggestive of a shift from the polymer's bulk (alternating gyroid) form to a surface parallel lamellar morphology in thin films, a result of interfacial interactions that propagate orientations of polymer domains parallel to the substrate surface.[52] As Figure 3d (left panel) demonstrates, the lamellar ordering persists for several L_0 periods, and for cases where $\theta_{w,s} > 70°$, we observed this morphology in films annealed for up to 12 h. Because PI is the lowest surface energy species in the ISO system, it necessarily resides at the free surface. This, in concert with block connectivity, is consistent with surface parallel lamellae having an internal ordering of I−S−O/O−S−I, as illustrated in Figure 5e and discussed in more detail later.

Figure 3c shows the film library after 2 h of annealing. This optical image shows a stable (lamellar) film on more hydrophobic
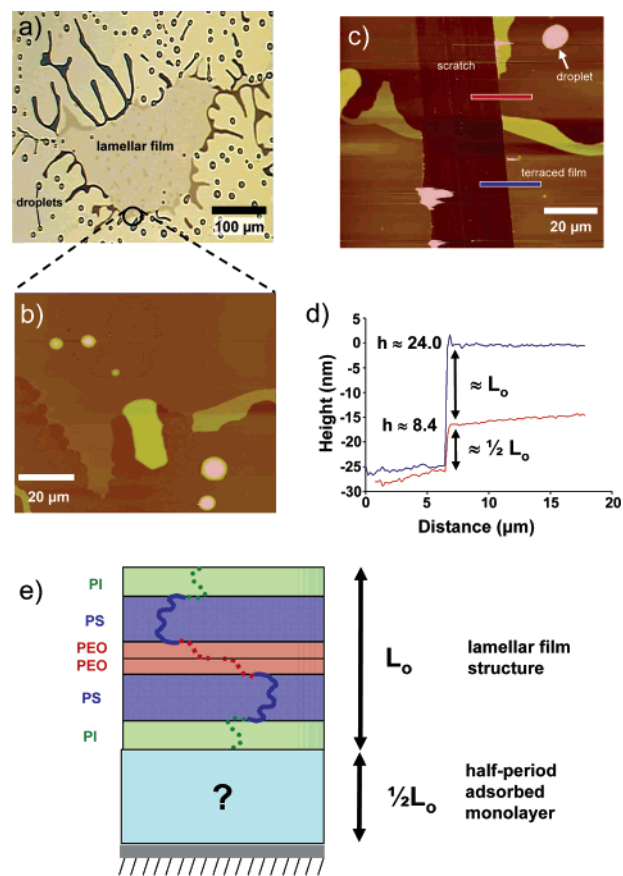
(52) Xu, T.; Hawker, C. J.; Russell, T. P. *Macromolecules* **2005**, *38* (7), 2802−2805.
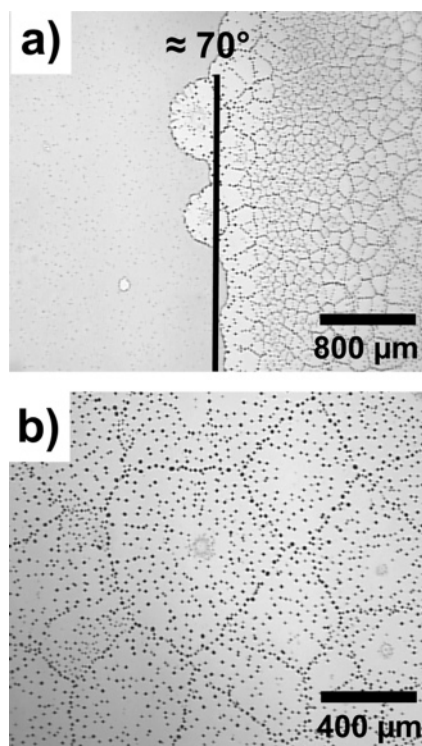
Figure 4. (a) Optical micrograph of polymer film following 8 h of annealing at 120 °C. The vertical line highlights the sharp transition between film wetting and dewetting, found at $\theta_{w,s} \approx 70°$. (b) Optical microscopy image of dewetted film at $\theta_{w,s} \approx 30°$ after 8 h of annealing at 120 °C. The dewetted structure is representative of film morphologies observed for $\theta_{w,s} < 70°$. The droplet pattern indicates "slippage" of the film, a key sign of autophobic wetting.

(higher $\theta_{w,s}$) substrates, and partial film dewetting when the substrate is more hydrophilic (lower $\theta_{w,s}$), shown in greater detail in Figure 3d (right panel). After 8 h of annealing, this trend persists, but film dewetting is apparently complete. Our observations indicate that dewetting does not occur until the sample is annealed for at least 1 h and appears to reach steady state after 3 h. As demonstrated in Figure 4a, the transition between the stable film and the dewetted region is quite sharp and occurs at $\theta_{w,s} \approx 70°$. Figure 4b shows a more detailed image of the dewetted ISO film morphology in a region where $\theta_{w,s} \approx 30°$. This micrograph shows droplet polygons that have resulted from the formation, growth, and impingement of holes as the film dewets;[31,37] a "snapshot" of this process after 2 h of annealing is seen in Figure 3d (left panel). In addition, the dewetted film morphology exhibits a distribution of droplets within the polygons. The radial arrangement of these droplets is likely due to "slippage" effects,[28,37,53,54] which can result when a film dewets from a compliant surface, e.g., an adsorbed polymer monolayer. This droplet structure is indicative of an autophobic dewetting process. Similar late-stage droplet morphologies were observed for all values of $\theta_{w,s} < 70°$.

To examine the film morphology and dewetting process further, we return our attention to observations made at shorter annealing times when the film exhibits partial dewetting for $\theta_{w,s} < 70°$. Figure 5 shows optical microscopy and AFM data from films after 1 h of annealing in an area where $\theta_{w,s} \approx 52°$. The optical micrograph in Figure 5a shows the coexistence between a terraced film and dewetted droplets at this level of annealing. This micrograph suggests that the dewetting front (at the edge of the

(53) Ajdari, A.; Brochardwyart, F.; Degennes, P. G.; Leibler, L.; Viovy, J. L.; Rubinstein, M. *Physica A* **1994**, *204* (1−4), 17−39.
(54) Reiter, G.; Khanna, R. *Phys. Rev. Lett.* **2000**, *85* (13), 2753−2756.

Figure 5. Film structures after short annealing times. (a) Optical microscopy image at $\theta_{w,s} = 52°$ after 1 h of annealing. The edges of this patch of terraced film form tendrils that have pinched droplets, indicative of slippage. (b) AFM topography micrograph at the edge of the film patch shown in part a. (c) AFM scratch test in region of film from part a. The red line indicates the location of a height cross section across the scratch and surface in contact with the dewetted droplets. The blue line indicates the location of a height cross section across the scratch and film surface prior to dewetting. (d) AFM cross section collected along the colored lines in part c. Step changes in height show transitions from surface of scratch to surface of wetting layer (red line) and surface of polymer film (blue line). (e) Cartoon of proposed film cross section. The structure of the adsorbed monolayer is discussed in the text.

film patch) exhibits build-up of higher, multiple period terraces, that narrow and then break off into droplets as the dewetting progresses. This process is likely related to the slippage phenomenon noted above. AFM topography micrographs along the dewetting front (see Figure 5b) reveal that terraces are 16 nm in height, and AFM phase images in this area (not shown) indicate that terraces lack lateral nanostructuring, again indicative of a surface parallel lamellar film microstructure. "Scratch" tests were used to resolve features of the film structure. For these tests, we used a razor blade to remove a strip of film. Subsequent AFM analysis of the edge of the scratch allows for determination of local variations in the film thickness using the exposed substrate as a reference. Scratch tests in the range of surface energy where the film is stable ($\theta_{w,s} > 70°$) allow us to conclude that the bulk of the film is supported by a monolayer that is approximately $L_0/2$ thick and that the structure exhibits an antisymmetric morphology. For ($\theta_{w,s} < 70°$), a different scenario results, as shown in parts c and d of Figure 5. In this case, the scratch runs through a patch of terraced film and an adjacent area exhibiting droplets (Figure 5c, AFM micrograph). Film heights were measured along the red (dewetted area) and blue (lamellar film) lines. As demonstrated by the cross-section data in Figure 5d,

and illustrated in Figure 5e, step heights along these lines indicate that both the film and dewetted droplets rest on a surface adsorbed monolayer that is $\approx L_0/2$ thick. This verifies that autophobic dewetting is occurring. Similar observations were made across the entire library where $\theta_{w,s} < 70°$. In addition, we note that AFM phase micrographs of the exposed wetting layer do not exhibit lateral structure.

To our knowledge, there are no previous reports of autophobic dewetting in ABC triblock thin films; however, the fact that autophobic dewetting is exhibited by an ABC system is not in itself surprising. As demonstrated in our work and other reports,[15,16,25] ABC films can exhibit adsorbed layers at the substrate, and as observed with diblock films,[18,19] such monolayers can create the entropic conditions necessary to drive autophobic behavior. What makes our observations unique is the strong dependence of the dewetting behavior on the substrate surface energy, and the sharp transition between autophobic dewetting and a stable film at a particular surface contact angle, i.e., $\theta_{w,s} \approx 70°$. If we apply the hypothesis of Sommer and Reiter[29,40] for the case of PEO homopolymers to our system, the behavior of our ISO triblock could entirely be due to changes in the conformational entropy of the monolayer induced by variations in the substrate interaction. However, if this were the case, we would find systematic changes in the thickness of the ISO monolayer along our library, but these were not observed. Moreover, measurements of the surface chemistry of the monolayer suggest that a purely entropic explanation is not adequate for our ISO triblock, and that *enthalpic* interactions can also play a significant role in the autophobic dewetting of this system. We discuss this analysis in more detail next.

For surface chemical analysis of the absorbed monolayer, we employed XPS and NEXAFS spectroscopy on a 9 nm thick ($\approx L_0/2$) ISO film, which was deposited on a surface energy library identical to that illustrated in Figure 3a. The film was annealed for 6 h at 120 °C. Measurements of the free surface of the film (hereafter "top" surface) were conducted on films residing on the substrate. NEXAFS analysis of the substrate/monolayer interface (hereafter "bottom surface") was enabled by peeling the film from the substrate, as described in the Experimental Section and Figure 2.

Figure 6 displays XPS data from the top surface of the ISO monolayer film library. Argon ion etching of the film allowed us to determine the film composition near the bottom surface. Figure 6a shows XPS survey scans of the film area where $\theta_{w,s} \approx 10°$. Binding energy peaks at 286, 533, and 744 eV were used to determine relative concentrations of carbon, oxygen, and silicon, respectively. Analysis of data acquired before etching (red curve) indicates that the top surface of the adsorbed monolayer is rich in the hydrocarbon blocks, i.e., PS and/or PI. The O and Si signals closely match SiO_2 stoichiometry, so they can be attributed to SiO_2 contamination resulting from wafer sectioning. After ion etching (blue curve) the oxygen signal cannot be accommodated by SiO_2 stoichiometry. Therefore, near the substrate the wetting layer is rich in the PEO block. This concentration profile is reasonable, since the PEO block is expected to segregate to the hydrophilic substrate in this region while lower surface tension hydrocarbon blocks will segregate to the free surface.

Figure 6b summarizes C and O mass fractions at the top surface as a function of $\theta_{w,s}$ along the library; these data were acquired from an unetched film. As $\theta_{w,s}$ decreases, the C mass fraction increases and the O mass fraction decreases. This indicates that the top surface is gradually enriched by hydrocarbon blocks as the substrate becomes hydrophilic, while PEO segments begin
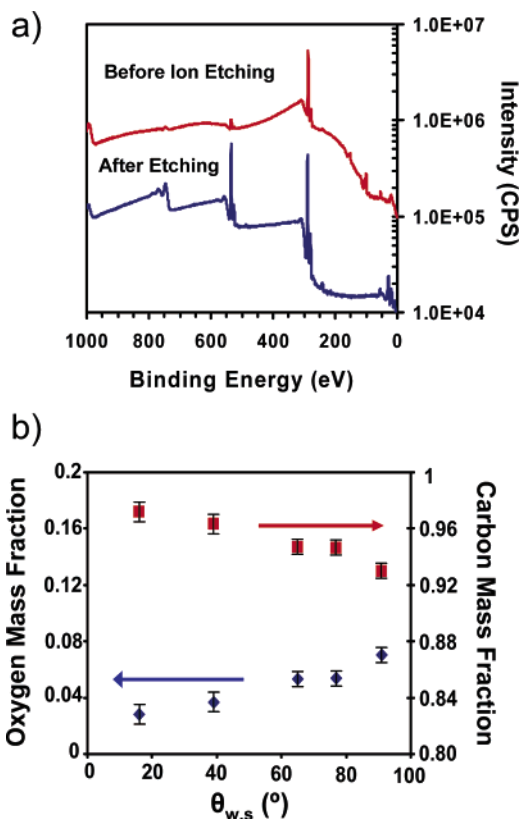
Figure 6. (a) XPS survey scan of polymer wetting layer at $\theta_{w,s} \approx 10°$ following 6 h of annealing at 120 °C. XPS sample-to-detector angle is 90°. The film is ≈ 9 nm thick. Red curve is scan prior to etching with argon ions. Blue curve is scan following 5 min of etching with argon ions. (b) XPS data of film similar to that in part a displaying oxygen and carbon mass concentrations on the top surface of the polymer wetting layer as a function of $\theta_{w,s}$. XPS sample-to-detector angle was 30°. Oxygen and carbon mass concentrations are indicated by blue and red points, respectively. Error bars represent 2 standard deviations.

to reside near the top surface as the substrate becomes more hydrophobic. Mass conservation in the film implies the reverse trend on the bottom surface of the monolayer, which is PEO rich at low $\theta_{w,s}$ and has increasing levels of hydrocarbon segments as the substrate becomes more hydrophobic.

NEXAFS spectroscopy (Figure 7) allows us to more directly examine the chemistry of the bottom surface of the polymer wetting layer and to resolve the relative concentrations of the two hydrocarbon blocks (PS and PI). Differentiation of the PS and PI carbon binding energy peaks is not possible using the non-monochromatic XPS source, while NEXAFS spectroscopy permits differentiation of all three segment types in the ISO copolymer, as demonstrated by spectra obtained from individual homopolymer samples in Figure 7a. Intensities of the 1s → π* peak at 285 eV are key to discriminating between the three polymer blocks. Linear combinations of these homopolymer spectra are used to determine the composition of heterogeneous systems,[51] like our ISO triblock. For example, Figure 7b displays the measured spectra data and calculated fit for the bottom surface of the ISO monolayer at $\theta_{w,s} = 79°$. The excellent agreement between these measured data and the fit is representative of the NEXAFS analyses along the entire monolayer film library. Figure 7c summarizes the molar compositions of PS and PEO segments as a function of $\theta_{w,s}$. As clearly demonstrated in this figure, the molar fraction of PS at the bottom surface of the monolayer increases as the substrate becomes more hydrophobic and varies from 44% ± 2% at $\theta_{w,s} \approx 10°$ to 79% ± 1% at $\theta_{w,s} \approx 88°$. In

a)

b)

c)
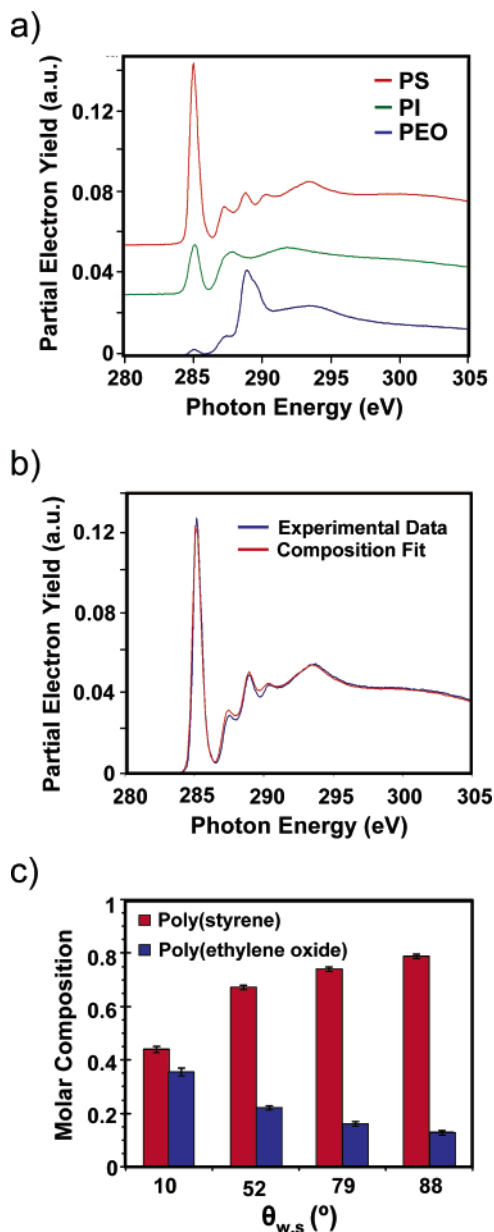
Figure 7. (a) NEXAFS carbon K-edge spectra for PS, PI, and PEO homopolymer thin films. (b) NEXAFS carbon K-edge spectra for the bottom surface of the ISO wetting layer at $\theta_{w,s} = 79°$ (blue curve) and a composition fit curve (red curve). The fitted data allow us to determine the molar composition of the film residing next to the substrate. (c) NEXAFS data from the bottom surface of the ISO monolayer showing PS and PEO composition as a function of $\theta_{w,s}$. The film was annealed for 6 h at 120 °C. The bottom surfaces were exposed using the carbon evaporation/PAA method described in the text. Error bars represent 1 standard deviation.

contrast, the molar fraction of PEO decreases as $\theta_{w,s}$ increases, varying from 35% $\pm$ 2% at $\theta_{w,s} \approx 10°$ to 14% $\pm$ 1% at $\theta_{w,s} \approx$ 88°.

Overall, the NEXAFS and XPS analyses demonstrate that the monolayer adjusts expression of the PI, PS, and PEO segments at both the top and bottom surfaces to accommodate substrate interfacial interactions. Accordingly, in addition to possible changes in conformation entropy, the monolayer certainly expresses measurable changes in its surface chemistry (and thus surface energy), and we believe that this segmental expression is essential to the autophobic dewetting behavior of this ISO system. In this sense, our understanding of the film behavior has developed into two general cases, which are illustrated in Figures
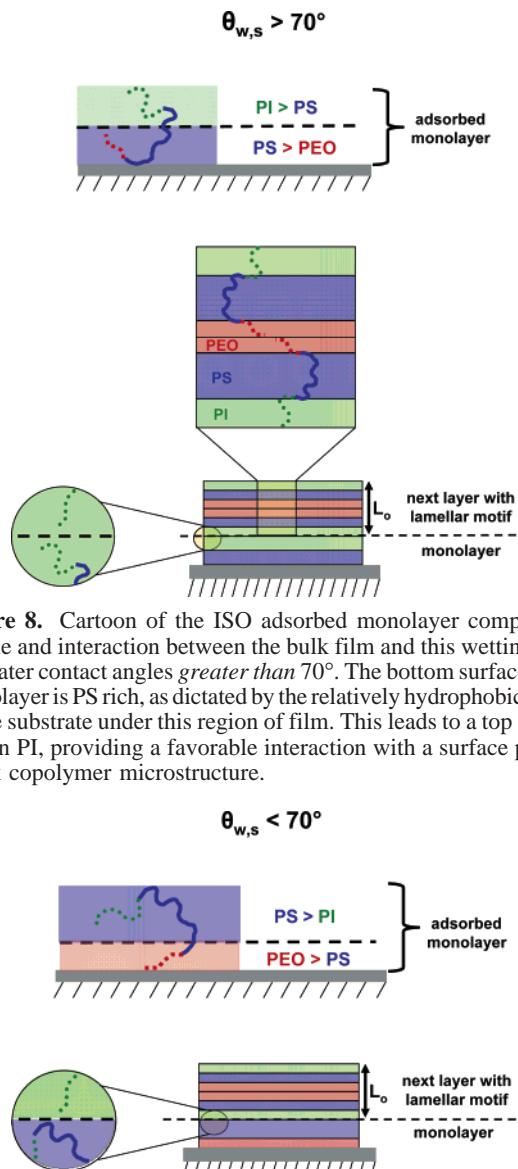
Figure 8. Cartoon of the ISO adsorbed monolayer composition profile and interaction between the bulk film and this wetting layer for water contact angles *greater than* 70°. The bottom surface of the monolayer is PS rich, as dictated by the relatively hydrophobic nature of the substrate under this region of film. This leads to a top surface rich in PI, providing a favorable interaction with a surface parallel block copolymer microstructure.

Figure 9. Cartoon of the ISO adsorbed monolayer composition profile and interaction between the bulk film and the wetting layer for water contact angles *less than* 70°. The bottom surface of the wetting layer is PEO rich, as dictated by the relatively hydrophilic nature of the substrate under this region of film. This leads to a PS-rich top surface, generating less favorable interaction with a surface parallel block copolymer microstructure bounded by PI "capping layers".

8 and 9. Inherent to this understanding is the observed inclination of our ISO triblock toward a surface parallel morphology in thin films, which is shown schematically in Figures 5e and 8. Figure 8 illustrates the case for more hydrophobic substrate regions, where $\theta_{w,s} > 70°$. $\theta_{w,s} \approx 70°$ corresponds to a substrate surface energy of approximately 40 mJ/m²,[17] which is close to the surface energy of PS (39 mJ/m²).[17] Thus, the substrate interacts favorably with the PS block in the monolayer, forcing PS toward the substrate. Conservation of mass then requires the top surface of the monolayer to become enriched with PI segments, which is an energetically favorable platform for the overlying surface parallel film. Hence, the film is stable in this regime. As shown in Figure 9, more hydrophilic substrates ($\theta_{w,s} < 70°$) preferentially attract PEO segments. This phenomenon results in a monolayer with a more PS-rich top surface, which is not as energetically favorable for an overlying lamellar film that express the PI block,

as shown in Figure 9. Additionally, it is worth noting that the annealing temperatures employed in this work (120 °C) are below the polymer's bulk order−disorder transition temperature. Thus, enthalpic considerations still govern the film's behavior, and the unfavorable interaction between PS in the monolayer and PI in the overlying film drives dewetting.

IV. Conclusions

Our use of gradient combinatorial libraries allows us to very systematically examine the effect of substrate surface energy on the morphology and stability of a poly(isoprene-*b*-styrene-*b*-ethylene oxide) triblock copolymer thin film. Our first conclusion is that over the range of substrate surface energy we considered the polymer shifts from its bulk alternating gyroid morphology to a surface parallel microstructure in thin film geometries. The observed lack of lateral features in the film suggests a surface parallel lamellar motif. The surface parallel ordering is anti-symmetric, meaning in part that the film is supported by a half-period monolayer residing at the substrate surface. Our second conclusion is that the system undergoes a surface-energy-dependent autophobic dewetting upon annealing. Films remain stable on more hydrophobic substrates where $\theta_{w,s} > 70°$ but undergo dewetting from the monolayer when $\theta_{w,s} < 70°$. XPS and NEXAFS measurements show that as the substrate changes from hydrophilic to hydrophobic, the bottom surface of the monolayer gradually changes from a majority of PEO segments to predominantly PS segments. As the amount and type of segments pinned at the substrate change, the top surface of the monolayer also changes in its chemical nature, and we believe that this is the deciding factor between a stable film and autophobic dewetting in our ISO system. Over hydrophobic substrates, the top of the monolayer is enriched with PI, which forms an energetically favorable platform for PI-capped lamellae, so the film is stable. In contrast, as the substrate becomes more hydrophilic, the top of the monolayer becomes enriched with PS, which is energetically unfavorable for lamellae, so dewetting from the monolayer occurs. Previous treatments of autophobic dewetting in polymer melts have concentrated on systems in which unfavorable entropic interactions between an absorbed monolayer and the rest of the film are the dominant factor, and most experimental work has focused exclusively on this effect. The dominant role of enthalpic interactions in autophobic dewetting of small molecules is well established, and previous considerations of polymer autophobic dewetting have not precluded enthalpic effects. However, our combinatorial mea-surements of a triblock copolymer film provide direct evidence that unfavorable enthalpic interfacial interactions can play a *dominant* role in polymer autophobic wetting behavior. To our knowledge, our observations represent the first experimental demonstration of this effect.

LA062707Q